Analyst

Accepted Manuscript

ROYAL SOCIETY OF CHEMISTRY

www.rsc.org/analyst

Cite this: DOI: 10.1039/c0xx00000x

www.rsc.org/xxxxxx

ARTICLE TYPE

Highly Stable Colorimetric Aptamer Sensor for Ochratoxin A through Optimizing the Sequence with the Covalent Conjugation of Hemin

Jayeon Lee[a,b] , Chang Hoon Jeon[a,b] , Sang Jung Ahn[c], and Tai Hwan Ha*[a,b]

Received (in XXX, XXX) Xth XXXXXXXXX 20XX, Accepted Xth XXXXXXXXX 20XX

DOI: 10.1039/b000000x

Optimization of hairpin DNA is introduced to detect Ochratoxin A (OTA) by chemically conjugating its cofactor, hemin, toward 5'-end. The newly designed OTA aptasensor showed enhanced stability and sensitivity, thereby lowering detection limit to ~ 1 nM level. Furthermore, optimal spacer for hemin conjugation was investigated for stable responses toward much diluted OTA solutions.

1.Introduction

Ochratoxin A (OTA) belongs to mycotoxins that are secreted from microorganisms such as *Aspergillus* and *Penicillium*[1]. As a secondary metabolite of the fungi strands, ochratoxin derivatives can survive eradication of the living fungi; OTA is chemically stable and has relatively long half-life (35.5 days in human)[2]. Therefore, it attracts research attention as a new threat for public health and is required to regulate due to potential bioterrorism. Since its producers grow easily not only in the stock of various grains like coffee, peanut, and rice but also in commercialized food systems like wine, bread, and even meat product[3], the detected levels in the developed countries are high enough to recruit research efforts to monitor its existence in various food systems[1b]. Cytotoxic effects of OTA are largely associated with the inhibition and activation of enzymes which are involved in protein synthesis and apoptosis[4]. OTA also exhibits immunosuppression activities such as reduction of immune organs[5], depression of antibody responses, alterations in immune cell activities[6], and modulation of cytokine production[7]. As such, regulatory limits for OTA have been prepared in many countries and several detection methods were already presented. Several popular methods are based on ELISA or immunoaffinity column followed by chromatography such as thin layer chromatography and HPLC[8]. However, those detection methods require a trained handler and sophisticated equipment, which make it a time consuming and expensive work to detect OTA.

Recently, the development of OTA-specific DNA aptamer sheds light on a new detection methodology of high sensitivity and accuracy[9], and several biosensors based on OTA aptamer have been reported since its discovery[10]. Among them, one of the most powerful scheme for OTA detection might be the accomplishment acquired by linking target-specific aptamer with a G-quadruplex sequence[11]; the G-quadruplexes from G-rich sequences are formed in the presence of potassium ions and hemins by forming noncovalent complex and can mimic the protein counterpart, horse radish peroxidase (HRP). In this scheme, the peroxidase activity of G-quadruplex is initially hindered by a hairpin structure, but the HRP activity is revived upon exposure to target molecules; besides OTA, several other hairpin structures for biosensor applications have been reported with a similar mechanism[12]. The sensing strategy seems to have many implications in aptamer biosensors since probing target molecules and signal transductions are accomplished sequentially in a single oligonucleotide, thereby simplifying the reaction scheme, which is beneficial for the field detection.

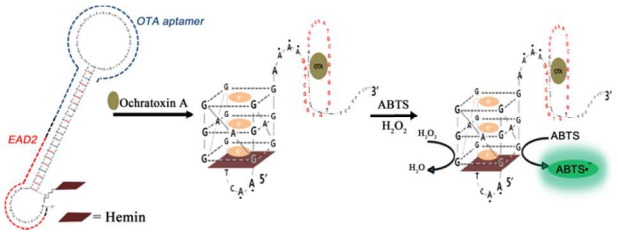

Fig.1 A schematic cartoon depicts a design of hemin-conjugated DNA hairpin that is used in this study, and its structural change upon recognition of OTA, which forms an active G-quadruplex; the red, blue, and black dashed lines in the left are denoting EAD2, OTA aptamer, and a spacer region, respectively.

Herein, we report the development of a simple optical sensing scheme for OTA aptasensor where hemin is covalently attached to the hairpin sequences, and an optimization on the overall sequence was attempted for better performance; in the presence of OTA, the stem of a hairpin is loosen to freely form G-quadruplex (EAD2) with covalently conjugated hemin, and expresses HRP activity (with the detection limit of several nM). As depicted in Fig. 1, a spacer region linking hemin to EAD2 (two dotted adenosines) and the other region connecting EAD2 and OTA aptamer (three dotted adenosines) are investigated for the sequence optimization. It has been already reported that the essential cofactor for G-quadruplex, hemin, could be covalently attached to the 3'-terminus of another G-quadruplex sequence (PS2M)[13], but the extension of the strategy toward another sequence (EAD2) has never been reported with actual target. Moreover, general consideration for the sequence design of the additional nucleotides that connect hemin with G-quadruplex sequences is also investigated.

2. Experimentals

2.1 Materials

Oligonucleotides were purchased from Bioneer Inc. (Daejeon, Korea) and used as received. 30% H_2O_2 was purchased from Daejung Chemicals & Metals Co. (Korea) and ABTS, hemin and all other chemicals were purchased from Sigma-Aldrich and used without purification.

Table 1. Designed OTA hairpin DNA(OHD) sequences

Name	Sequence (5' to 3')
OHD 1[a]	CTGGGAGGGAGGGAGGGAAAAGATCGGGTGTGGGTGGCGTAAAGGGAGCATCGGACACCCGATCTTTTCCCTCCC
OHD 2	***AA***CTGGGAGGGAGGGAGGGAAAAGATCGGGTGTGGGTGGCGTAAAGGGAGCATCGGACACCCGATCTTTTCCCTCCC
OHD 3	***AAAAA***CTGGGAGGGAGGGAGGGAAAAGATCGGGTGTGGGTGGCGTAAAGGGAGCATCGGACACCCGATCTTTTCCCTCCC
OHD 4	***TTTTT***CTGGGAGGGAGGGAGGGAAAAGATCGGGTGTGGGTGGCGTAAAGGGAGCATCGGACACCCGATCTTTTCCCTCCC

[a] OHD 1 was prepared for both conjugated and free DNA.

2.2 Hemin conjugation

NHS ester of hemin, Hemin-$(NHS)_2$, was prepared by standard synthetic scheme[13] using DCC as carboxylate activating reagent at room temperature in DMF solution followed by a separation step with silica gel column chromatography (TLC image of Fig. 2). The purified Hemin-$(NHS)_2$ was aliquoted in 1.5ml tubes, stored in refrigerator (-80 °C), and used in the next step without further treatment. The structure was confirmed by NMR and ESI-MS. For the hemin functionalization of target sequences, typically 250 μM amino-functionalized DNA (OTA hairpin DNA, OHD) in 20mM DIPEA (20 μL) was mixed with 40-fold molar excess of Hemin-$(NHS)_2$ dissolved in DMSO (20 μL). After 24 hours incubation for amide coupling, 2.5 volume of icy absolute ethanol and 0.1 volume of sodium acetate were added to the mixture and incubated for another 1 hour. The DNA precipitate was separated by centrifugation (15000 rpm, 15min.), redissolved with water (500 μL), and a purification procedure was repeated four times with QiaQuick Nucleotide Removal Kit (Qiagen, Germany). Both 1:1 free OHD-hemin mixture and OHD-hemin conjugates were prepared in water with same concentration and their absorbance spectra were compared to confirm the 1:1 molar ratio of the conjugate. The extinction coefficients of DNA at 260nm were supplied by IDT and that of hemin at 407nm was acquired from a previous report.[14]

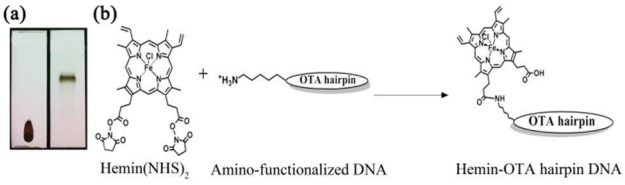

Fig.2 (a) Hemin and purified Hemin-$(NHS)_2$ (left to right in TLC images) (b) Conjugation of OTA hairpin oligonucleotide (OHD) with purified Hemin-$(NHS)_2$

2.3 Enzymatic Assays for OTA-hairpin using ABTS substrate

Prior to use all sample solutions, they were heated up to 95°C for 5min in advance and cooled down to room temperature, and then dissolved in 100 mM sodium phosphate buffer (pH 6.7) including 200 mM NaCl, 20 mM $MgCl_2$ and 5 mM KCl. Enzymatic substrates (5 mM ABTS and 50 mM H_2O_2) were prepared in the same buffer and stood at least 2 hours before use.

Kinetic studies for all complexes were investigated by observation of time-dependent absorbance changes of peroxidase substrate, ABTS, at 405nm. In detail, OHD oligonucleotides were premixed with OTA and hemin for 30 min for the restructuring, before ABTS/H_2O_2 mixture was added. The concentrations of oligonucleotides were in the range of 10 nM (for OHD-hemin conjugates) to 100 nM (for free OHD). In each OTA concentration, absorbance changes were recorded for 5 min and initial velocities of OHD at each OTA concentration were calculated from its plot of absorbance changes versus time course. Four models with different number of nucleotides-tail were used for OHD- hemin conjugation.

In order to estimate the Gibbs free energy changes of hairpin formation, OligoAnalyzer program from Interaged DNA Technologies (IDT, www.eu.idtdna.com) was employed. The binding free energy between hemin and EAD2 was estimated by acquiring binding isotherms (see ESI) and that between OTA and OTA aptamer sequence was estimated from the dissociation constant that had been acquired in the previous SELEX procedure[9]. All the free energies were calculated at 298 K in the given ionic strength of the buffer used.

3. Results and Discussion

Among aqueous aptasensor platforms, DNA hairpin structures employing G-quadruplex sequence on the one end as a reporting unit have been highly popular owing to their simple scheme and higher sensitivities. These G-quadruplex hairpins are proved to be successful for detecting lysozyme[12], ATP[15], AMP[16], oncogenes for breast cancer (BRCA1)[17], and OTA[11]. Before investigating the effect of hemin conjugation, the OTA sensing capability of the reported OTA aptasensor (OHD_0) was revised. In the previous OTA sensing sequence linked with G-quadruplex, its responses toward nanomolar concentrations of OTA have shown rather lower sensitivities as the OTA concentration increases, which is inconsistent with the previous observation. As shown in the ESI, the sensing capability of hairpin DNA employing exactly the same sequence in the previous report was quite disappointing in that the absorbance increases only gently as OTA concentration increases, even at relatively high DNA concentration (500 nM); at a lower concentration (i.e., 50 nM), the original sequence largely failed to show proportional increase of HRP signals versus OTA concentrations (see Fig 4(a)). In an attempt to resolve the discrepancies, the original sequence was closely scrutinized, and we found that the EAD2 shares two oligonucleotides with the OTA aptamer sequence as shown in Fig 3(a). In addition, high background HRP activities at the relatively low concentrations of OTA suggests that the hairpin formed by twelve base pairs is not much strong enough to maintain the stem-loop structure against the spontaneous formation of G-

quadruplex by hemin.

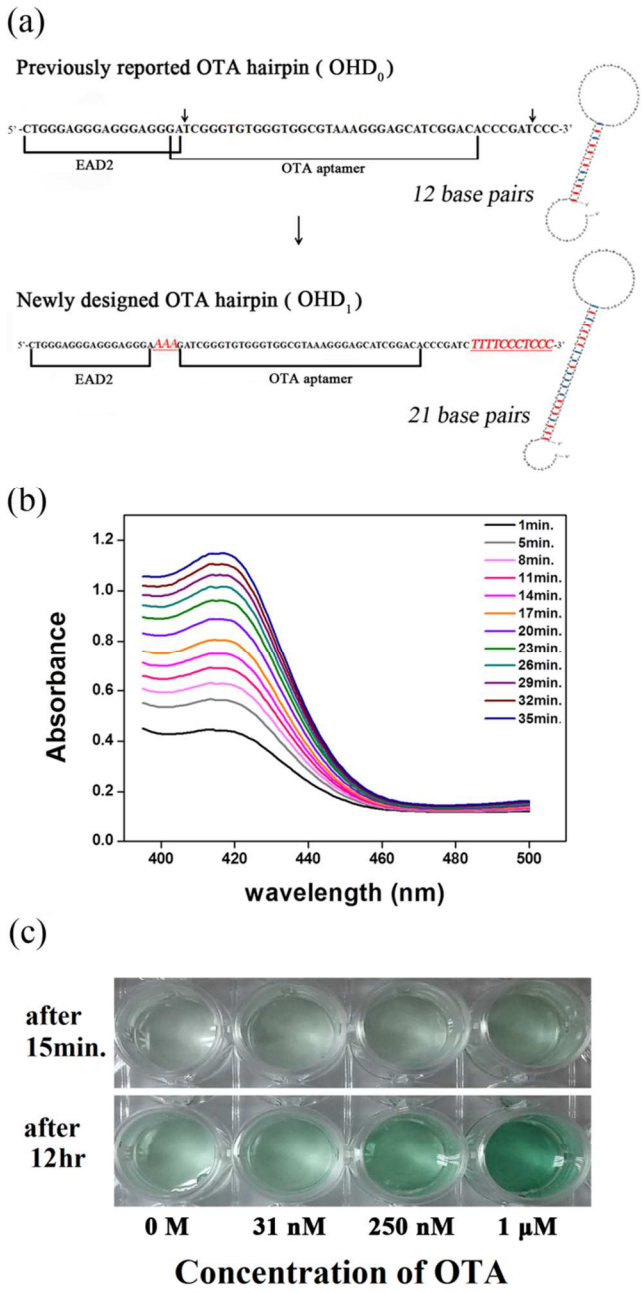

Fig.3 (a) A comparison of previous reported hairpin structure versus newly designed one. (b) Time-dependent absorbance changes of OHD_1 (100 nM, hemin 300 nM, OTA 250 nM) and (c) OTA-dependent color changes 15 min and 12 hr after the addition of ABTS/H_2O_2 (OHD_1 100 nM, hemin 300 nM).

Motivated by these observations, a new sequence design, OHD_1, has been introduced in order to enhance the stability of the hairpin thereby to fortify the reproducibility of the aptasensor. In the first place, we separated two functional sequences by a spacer sequence of three adenosines, which was intended to eliminate possible interferences that one structure might exert to the other, or vice versa (see Fig 3(a)). In determining the spacer sequences, guanosine or cytidine residues were avoided not to interfere the restructuring of a G-rich EAD2 sequence. Second, the stem part has been elongated from 12 base pairs in OHD_0 to 21 base pairs in order to evade premature melting of the hairpin; among the 21 base pairs, 8 base pairs were intended to block EAD2 part while 10 base pairs to hinder the OTA aptamer sequence. By the elongation of the stem part, the stability of OHD_1 hairpin is estimated to reach -24.6 kcal/mol of free energy change ($\Delta G^\circ_{hairpin}$) so that the hairpin structure has greater stability than the original hairpin (-17.2 kcal/mol). In the meantime, the free energy change for the formation of G-qudruplex with hemin (ΔG°_{EAD2}) is estimated to be -8.3 kcal/mol, according to a control experiment to find the binding constant between EAD2 and hemin (see ESI), while the free energy change between OTA and the OTA aptamer sequence (ΔG°_{OTA}) is estimated to be -16.2 kcal/mol in the initial SELEX process[9]; for ΔG°_{OTA}, self-folding energy (-7.4 kcal/mol) is added to the binding energy (-8.8 kcal/mol) observed experimentally. Keeping these parameters in mind, it seems that the half of the hairpin would be released to construct the reporting G-quadruplexes because the stability of the hairpin ($\Delta G^\circ_{hairpin}$, -24.6 kcal/mol) is quite comparable to the interaction energies (the sum of ΔG°_{EAD2} + ΔG°_{OTA}, -24.5 kcal/mol). Third, in addition to the elongation of the hairpin, the enzymatic cofactor, hemin, was in advance conjugated at the 5' end of OHD_1 to eliminate the dependence on its concentration over the enzymatic activities and to simplify the detection process. Compared to an exogenous addition, the hemin tethering seems to enhance the responsibility toward OTA (or to provide a lower free energy on the G-quadruplex formation change than -8.3 kcal/mol). In fact, another G-quadruplex sequence (PS2.M) that was chemically conjugated to hemin showed enhanced stability and a lower background signal[13].

The newly designed OHD_1 sequence demonstrated a comparable HRP activity to OHD_0 as shown in Fig. 3(b) even though a longer stem was employed. Moreover, in contrast to OHD_0, it was successful to detect the dependence on OTA concentrations with naked eyes as shown in Fig. 3(c). Nevertheless, the direct usage of the color table for the determination of OTA contents seems quite limited with the current peroxidase substrate (ABTS/H_2O_2), since the typical green color of ABTS/H_2O_2 also develops in the absence of OTA, due to weak HRP activity of hemin itself. Therefore, UV/Vis absorbance measurements for lower OTA concentrations have been thoroughly used to estimate the enzymatic activities and reproducibility of OHD derivatives.

In Fig 4(a), enzymatic reaction velocities of a few OHD derivatives were plotted against OTA concentrations in logarithmic scale while the linear plot is provided in the ESI. As mentioned in the above, OHD_0 at 50 nM largely failed to show any meaningful dependence on OTA concentrations with large experimental deviations, while the activities of the newly designed hairpin show fair dependence on the amount of OTA (see Fig. 4(a)). When the hemin addition was adjusted into one to one correspondence to the concentration of OHD_1 (50 nM), the HRP activity appeared but showed weak dependence on OTA concentrations as shown in Fig 4(a). With more addition of hemin (150 nM), higher HRP activities were observed in all ranges of OTA concentrations, revealing the feasible melting of the hairpin. However, the early turn-on of HRP activity at lower concentrations of OTA was also observed, suggesting that spontaneous melting of OHD_1 dominates in the signal and seems

to constitute the major background noise in other concentrations, too.

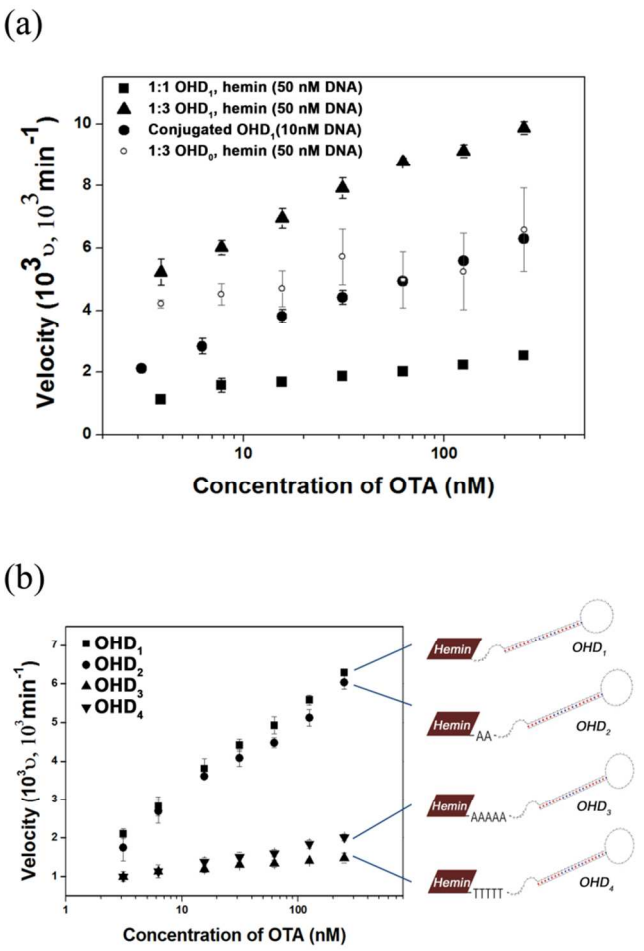

Fig.4 (a) Comparison of enzymatic velocity plots of three different states of OHD_1 and OHD_0; 50 nM OHD_1 and hemin (1:1) / 50 nM OHD_1 and 150 nM hemin (1:3) /10 nM hemin-conjugated OHD_1/ 50nM OHD_0 and 150 nM hemin (1:3) with a confidence level of 2σ. (b) Velocities of four hemin conjugated OHDs with different 5'-end sequences ([OHD_x] = 10 nM) with a confidence level of 2σ.

On the other hand, with hemin tethering, the hairpin DNA (*hem*-OHD_1) shows similar HRP activity in response to OTA (in terms of slope and enzymatic velocity) with those of uncoupled hairpins at 50 nM, even at a lower hairpin concentration (10 nM). Although we could not observe the velocity dependence on OTA concentrations at 10 nM OHD_1 with 30 nM hemin, *hem*-OHD_1 demonstrated good linearity over the OTA concentrations. The detection limit was observed to go down to ~1 nM level (2σ-confidence level) at 10 nM *hem*-OHD_1 and demonstrated enhanced reproducibility with low background noise compared to OHD_1 and OHD_0. Relatively low background noise in *hem*-OHD_1 might be attributed to the fact that hemin itself possesses weak HRP activity[18] since the reaction core of HRP activity is the hemin stacked by G-tetrad. Therefore, hemin tethering of the current OHD_1 sequence seems advantageous in detecting OTA at a very low concentration; employing small amount of *hem*-OHD_1 might evade the use of excessive and interfering free hemin.

As mentioned in the above, the free energy change of non-conjugated hairpin ($\Delta G^{\circ}_{hairpin}$) is designed to have a comparable value to the sum of the ΔG°_{EAD2} and ΔG°_{OTA}, such that only a portion of HRP activity will be revived in the presence of equal amount of OTA. Speculating the effect of hemin tethering on the thermodynamics, ΔG°_{EAD2} can be further lowered so that the hairpin melting in response to OTA could be more feasible without exogenous addition of hemin, which will result in easy turn-on of HRP activity toward OTA or higher background noise regardless of OTA contents. Conversely, covalent immobilization on oligonucleotides through amide bonding might hinder them from forming the optimized G-quadruplex structure by loss of freedom in molecular orientation, where ΔG°_{EAD2} will be raised or apparently resistant toward G-quadruplex formation in response to OTA. Among these two contradictable trends, easy turn-on tendency seems predominant when the HRP activity of *hem*-OHD_1 (10 nM) in the absence of OTA was compared with the value of OHD_1 (50 nM). The blank activity (enzymatic velocity, υ) with *hem*-OHD_1 was estimated to be $0.5x10^{-3}$ min^{-1} while $2.5x10^{-3}$ min^{-1} and $0.4x10^{-3}$ min^{-1} for OHD_1 with hemin of 150 nM and of 50 nM, respectively. Slightly faster HRP activity in *hem*-OHD_1 even at a lower concentration (10 nM) suggests that favorable and consistent G-quadruplex formation was accomplished by hemin tethering.

Guided by these observations, we further modified hairpin sequences in order to optimize the distance between hemin and the adjacent EAD2 sequence. A few nucleotides were added onto the EAD2 tail in 5'-position and the effects were investigated whether more flexible spacer between EAD2 and hemin contributes to activity of OHD aptasensor; their HRP activities *vs.* OTA concentration were monitored in comparison to the *hem*-OHD_1 sequence. As shown in Fig. 4(b), the longer is the additional spacer, the lower activity was observed and background signal was also decreased; *hem*-OHD_2 which has additional two adenosine spacers showed almost the same response as in OHD_1 while the activity drastically dropped with the spacer of five nucleotides. The observed spacer dependence might be attributed to the G-quadruplex structure itself of EAD2 with hemin, as depicted in Fig. 1; four guanines interact to form a planar tetrad and at least three of these tetrads are stacked to form a G-quadruplex, and then hemin is positioned on the top or under the bottom of this structure. Under the current scheme, hemin is located in the vicinity of 5'-end of G-quadruplex forming a lid to cover the guanine tetrad. Since the lower background signals in longer spacers imply the less complex formation between EAD2 and hemin, additional spacer tends to destabilize the G-quadruplex structure (or thus to lead the OHD to remain in stem-loop state). Therefore, it appears that a 'tight lid' is rather favored for the formation of EAD2 G-quadruplex. Moreover, the spacer dependence on HRP activity seems to enable one to tune the G-quadruplex formation precisely by regulating its length.

4. Conclusion

An aptasensor for OTA detection has been described by redesigning hairpin structure, thereby enabling it to have more stable stem-loop structure. Furthermore, the essential enzymatic cofactor, hemin, was chemically conjugated to the aptasensor in order to facilitate the G-quadruplex formation or to avoid using excessive hemin. The hairpin structure bearing EAD2 sequence at 5'-end played a colorimetric reporting beacon successfully, in

response to the restructuring of the adjacent OTA-binding sequence. With higher stability, the aptasensor showed rather consistent and stable HRP activities in proportion to the amount of OTA present in sample solutions with low background signal. It is envisioned that this design scheme will be applicable to other aptasensor design as a universal colorimetric or fluorometric detection mechanism for a wide range of hazardous materials.

This work was supported by grants of Korea Research Foundation (NRF-2012R1A1A2020074 and NRF-2010-0020840) and KRIBB initiative programs.

Notes and references

[a] *Nanobiotechnology (Major), School of Engineering, University of Science & Technology Centre, Daejeon 305-806, Republic of Korea. Fax: 82 42 879 8596; Tel: 82 42 860 4272; E-mail: taihwan@kribb.re.kr*

[b] *Research center of integrative cellolomics, Korea Research Institute of Bioscience and Biotechnology (KRIBB), Daejeon 305-806, Republic of Korea. Fax: 82 42 879 8596; Tel: 82 42 860 4272; E-mail: taihwan@kribb.re.kr*

[c] *Center for Nano-Imaging Technology, Division of Industrial Metrology, Korea Research Institute of Standards and Science (KRISS), Yuseong-gu, Daejeon 305-340, Republic of Korea*

† Electronic Supplementary Information (ESI) available: [Miscellaneous data including acquisition of dissociation constant between EAD2 and hemin by titration are provided in the ESI]. See DOI: 10.1039/b000000x/

‡ Footnotes should appear here. These might include comments relevant to but not central to the matter under discussion, limited experimental and spectral data, and crystallographic data.

1. (a) Van Der Merwe, K. J.; Steyn, P. S.; Fourie, L.; Scott, D. B.; Theron, J. J., Ochratoxin A, a Toxic Metabolite produced by Aspergillus ochraceus Wilh. *Nature* **1965,** *205* (4976), 1112-1113; (b) FAO/WHO, j., safety evaluation of certain mycotoxins in food. In *Prepared by 56th Meeting of the Joint FAO/WHO expert committee on Food Additives(JECFA)*, International Programme on Chemical Safety: World Health Organization, 2001; pp 281-415.

2. Studer-Rohr, I.; Schlatter, J.; Dietrich, D. R., Kinetic parameters and intraindividual fluctuations of ochratoxin A plasma levels in humans. *Arch Toxicol* **2000,** *74* (9), 499-510.

3. (a) Tsubouchi, H.; Yamamoto, K.; Hisada, K.; Sakabe, Y.; Udagawa, S.-i., Effect of roasting on ochratoxin A level in green coffee beans inoculated with Aspergillus ochraceus. *Mycopathologia* **1987,** *97* (2), 111-115; (b) Boudra, H.; Le Bars, P.; Le Bars, J., Thermostability of Ochratoxin A in wheat under two moisture conditions. *Applied and Environmental Microbiology* **1995,** *61* (3), 1156-8; (c) Battilani, P.; Pietri, A., Ochratoxin a in Grapes and Wine. *European Journal of Plant Pathology* **2002,** *108* (7), 639-643; (d) Losito, I.; Monaci, L.; Palmisano, F.; Tantillo, G., Determination of ochratoxin A in meat products by high-performance liquid chromatography coupled to electrospray ionisation sequential mass spectrometry. *Rapid Communications in Mass Spectrometry* **2004,** *18* (17), 1965-1971.

4. (a) Creppy, E. E.; Størmer, F. C.; Kern, D.; Röschenthaler, R.; Dirheimer, G., Effects of ochratoxin a metabolites on yeast phenylalanyl-tRNA synthetase and on the growth and in vivo protein synthesis of hepatoma cells. *Chemico-Biological Interactions* **1983,** *47* (2), 239-247; (b) Assaf, H.; Azouri, H.; Pallardy, M., Ochratoxin A Induces Apoptosis in Human Lymphocytes through Down Regulation of Bcl-xL. *Toxicological Sciences* **2004,** *79* (2), 335-344.

5. Boorman, G. A.; Hong, H. L.; Dieter, M. P.; Hayes, H. T.; Pohland, A. E.; Stack, M.; Luster, M. I., Myelotoxicity and macrophage alteration in mice exposed to ochratoxin A. *Toxicology and Applied Pharmacology* **1984,** *72* (2), 304-312.

6. Müller, G.; Burkert, B.; Rosner, H.; Köhler, H., Effects of the mycotoxin ochratoxin A and some of its metabolites on human kidney cell lines. *Toxicology in Vitro* **2003,** *17* (4), 441-448.

7. Lea, T.; Steien, K.; Størmer, F., Mechanism of ochratoxin A-induced immunosuppression. *Mycopathologia* **1989,** *107* (2-3), 153-159.

8. (a) Barna-Vetró, I.; Solti, L.; Téren, J.; Gyöngyösi, Á.; Szabó, E.; Wölfling, A., Sensitive ELISA Test for Determination of Ochratoxin A. *Journal of Agricultural and Food Chemistry* **1996,** *44* (12), 4071-4074; (b) Matrella, R.; Monaci, L.; Milillo, M. A.; Palmisano, F.; Tantillo, M. G., Ochratoxin A determination in paired kidneys and muscle samples from swines slaughtered in southern Italy. *Food Control* **2006,** *17* (2), 114-117.

9. Cruz-Aguado, J. A.; Penner, G., Determination of Ochratoxin A with a DNA Aptamer. *Journal of Agricultural and Food Chemistry* **2008,** *56* (22), 10456-10461.

10. (a) Bonel, L.; Vidal, J. C.; Duato, P.; Castillo, J. R., An electrochemical competitive biosensor for ochratoxin A based on a DNA biotinylated aptamer. *Biosensors and Bioelectronics* **2011,** *26* (7), 3254-3259; (b) Barthelmebs, L.; Jonca, J.; Hayat, A.; Prieto-Simon, B.; Marty, J.-L., Enzyme-Linked Aptamer Assays (ELAAs), based on a competition format for a rapid and sensitive detection of Ochratoxin A in wine. *Food Control* **2011,** *22* (5), 737-743; (c) Hun, X.; Liu, F.; Mei, Z.; Ma, L.; Wang, Z.; Luo, X., Signal amplified strategy based on target-induced strand release coupling cleavage of nicking endonuclease for the ultrasensitive detection of ochratoxin A. *Biosensors and Bioelectronics* **2013,** *39* (1), 145-151.

11. Yang, C.; Lates, V.; Prieto-Simón, B.; Marty, J.-L.; Yang, X., Aptamer-DNAzyme hairpins for biosensing of Ochratoxin A. *Biosensors and Bioelectronics* **2012,** *32* (1), 208-212.

12. Teller, C.; Shimron, S.; Willner, I., Aptamer−DNAzyme Hairpins for Amplified Biosensing. *Analytical Chemistry* **2009,** *81* (21), 9114-9119.

13. Thirstrup, D.; Baird, G. S., Histochemical Application Of A Peroxidase DNAzyme with a Covalently Attached Hemin Cofactor. *Anal Chem* **2010,** *82* (6), 2498-2504.

14. Uc, A.; Stokes, J. B.; Britigan, B. E., Heme transport exhibits polarity in Caco-2 cells: evidence for an active and membrane protein-mediated process. *American Journal of Physiology - Gastrointestinal and Liver Physiology* **2004,** *287* (6), G1150-G1157.

15. Freeman, R.; Liu, X.; Willner, I., Chemiluminescent and Chemiluminescence Resonance Energy Transfer (CRET) Detection of DNA, Metal Ions, and Aptamer–Substrate Complexes Using Hemin/G-Quadruplexes and CdSe/ZnS Quantum Dots. *Journal of the American Chemical Society* **2011,** *133* (30), 11597-11604.

16. Pelossof, G.; Tel-Vered, R.; Elbaz, J.; Willner, I., Amplified Biosensing Using the Horseradish Peroxidase-Mimicking DNAzyme as an Electrocatalyst. *Analytical Chemistry* **2010,** *82* (11), 4396-4402.

17. Shimron, S.; Wang, F.; Orbach, R.; Willner, I., Amplified Detection of DNA through the Enzyme-Free Autonomous Assembly of Hemin/G-Quadruplex DNAzyme Nanowires. *Analytical Chemistry* **2011,** *84* (2), 1042-1048.

18. Travascio, P.; Li, Y.; Sen, D., DNA-enhanced peroxidase activity of a DNA aptamer-hemin complex. *Chemistry & Biology* **1998,** *5* (9), 505-517.

5

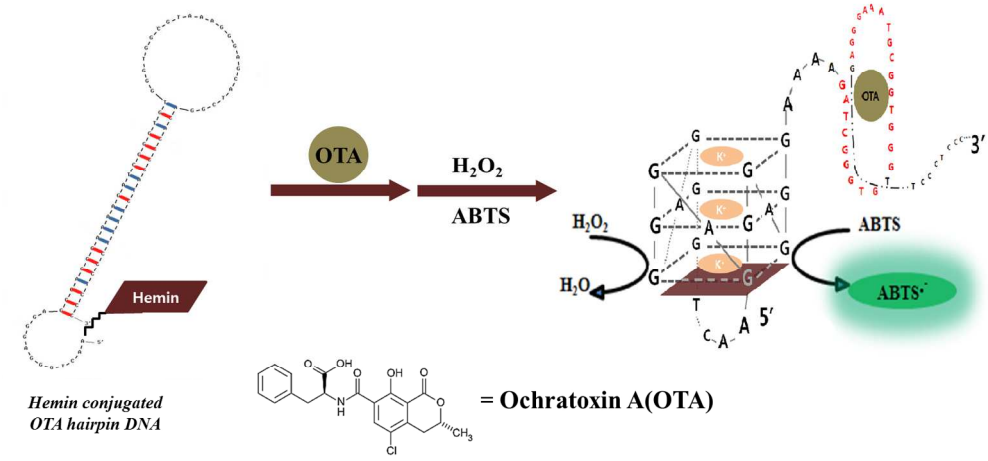

254x124mm (300 x 300 DPI)